Interplay between Turing Mechanisms can Increase Pattern Diversity

Shai Kinast,[1] Yuval R. Zelnik,[1] Golan Bel,[1,*] and Ehud Meron[1,2]
[1]Department of Solar Energy and Environmental Physics, Blaustein Institutes for Desert Research, Ben-Gurion University of the Negev, Sede Boqer Campus 84990, Israel
[2]Department of Physics, Ben-Gurion University, Beer Sheva, 84105, Israel

(Received 2 November 2013; revised manuscript received 18 December 2013; published 20 February 2014)

We use the context of dryland vegetation to study a general problem of complex pattern-forming systems: multiple pattern-forming instabilities that are driven by distinct mechanisms but share the same spectral properties. We find that the co-occurrence of two Turing instabilities when the driving mechanisms counteract each other in some region of the parameter space results in the growth of a single mode rather than two interacting modes. The interplay between the two mechanisms compensates for the simpler dynamics of a single mode by inducing a wider variety of patterns, which implies higher biodiversity in dryland ecosystems.

DOI: 10.1103/PhysRevLett.112.078701 PACS numbers: 89.75.Kd, 05.45.-a, 87.23.-n

The instabilities of uniform states in complex pattern-forming systems can be driven by two or more independent physical mechanisms. An illuminating example is vegetation pattern formation in water-limited systems (drylands). There is increasing evidence that dryland landscapes can self-organize to form spatial vegetation patterns even in fairly uniform regions [1,2]. Vegetation pattern formation is driven by positive feedbacks between local vegetation growth and water transport towards the growing vegetation. The depletion of water in the vicinity of the growing vegetation inhibits the growth there and promotes nonuniform vegetation growth [3]. At least three mechanisms of water transport can be distinguished: overland water flow induced by higher infiltration rates in denser vegetation patches ("infiltration feedback"), water conduction by laterally extended root zones that further extend as the plants grow ("root-augmentation feedback"), and fast soil-water diffusion relative to biomass expansion, in conjunction with strong water uptake by confined root zones ("uptake-diffusion feedback").

The instabilities induced by the different feedbacks all share the same spectral properties; that is, they all lead to monotonically growing modes that have the same spatial symmetry, a finite-wave-number mode in 1d (Fig. 1), or in 2d, the simultaneous growth of three modes with wave-vector directions $2\pi/3$ apart that yield hexagonal patterns. However, the modes that grow at these instabilities, and, consequently, the patterns that emerge, differ in the relative biomass-water distributions. The infiltration feedback acts to increase the soil-water content in patches of denser biomass, and, therefore, leads to in-phase biomass-water patterns [4]. By contrast, the root-augmentation feedback and the uptake-diffusion feedback act to deplete the soil-water content in denser biomass patches because of the higher water uptake, and, therefore, lead to antiphase biomass-water patterns [5].

Although the three feedbacks represent independent mechanisms of vegetation pattern formation, they are related to one another in the sense that varying the strength of one feedback may affect the strength of a different feedback. As a consequence, codimension-two points can be identified where two instabilities induced by distinct mechanisms coincide. The interplay between two co-occurring instabilities has been studied extensively for cases where the growing modes differ in their spectral properties (as dictated by the eigenvalues of the linear problem), i.e., either in their growth form, monotonic or oscillatory, or in their spatial symmetry, or in both. Such co-occurring instabilities are known as "codimension-two bifurcations" (see comment [6]). An illustrative example is the Hopf-Turing bifurcation in which a spatially periodic mode grows monotonically in time along with a uniform mode that grows in an oscillatory manner [7,8]. Another example is the growth of two surface-wave modes that have different spatial symmetries [9,10].

The interplay between two pattern-forming instabilities that share the same spectral properties, however, has not been studied. The reason may be the fairly simple pattern-forming systems that have been considered in model studies, which do not capture more than one mechanism for any instability, or to the focus on a single field, rather than on the relations between two independent fields, in empirical studies.

In this Letter, we use dryland vegetation as a case model for studying the behavior near a codimension-two point where two instabilities sharing the same spectral properties but driven by distinct mechanisms coincide. We focus on the infiltration and uptake-diffusion feedbacks in 1d, which both lead to finite-wave-number stationary instabilities but result in distinct patterns, in-phase and antiphase, respectively. Surprisingly, we find that the instability at this point is a codimension-one bifurcation that leads to the growth of

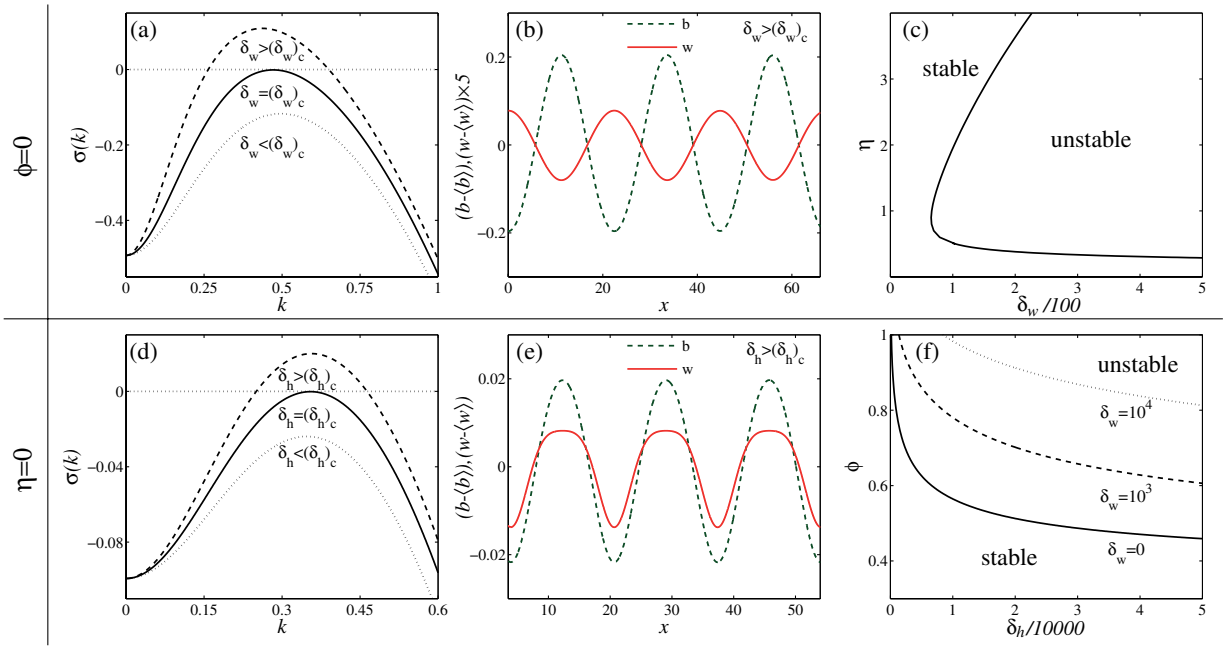

FIG. 1 (color online). Nonuniform stationary instabilities of uniform vegetation driven by the uptake-diffusion feedback ($\phi = 0$) (a),(b),(c) and by the infiltration feedback ($\eta = 0$) (d),(e),(f). Panels (a) and (d) show the growth rates $\sigma(k)$ of periodic perturbations with wave numbers k below (dotted line), at (solid line), and beyond (dashed line) the instabilities. Panels (b) and (e) show the antiphase and in-phase patterns the instabilities lead to, and panels (c) and (f) show the instability thresholds in the planes spanned by the parameters that control the instabilities. The three lines in panel (f) correspond to different values of δ_w as indicated in the figure; although $\eta = 0$, the instability threshold depends on the soil-water diffusivity. In panel (c), there is only one curve because for $\phi = 0$ the instability threshold is independent of the water transport coefficient, δ_h. Parameters for panels (a),(b): $\phi = 0$, $\eta = 0.9$, and $\delta_w = 70$. Parameters for panels (d),(e): $\eta = 0$, $\delta_w = 0$, $\phi = 0.9$, and $\delta_h = 400$.

a single mode that is neither in-phase nor antiphase. Nevertheless, the instability does contain information about the two distinct modes—the band of stable periodic solutions that appear beyond the instability point describes a family of stationary periodic patterns ranging continuously from in-phase to antiphase patterns. This behavior is unlike codimension-two bifurcations, which only show the distinct modes and combinations thereof (e.g., mixed-mode patterns) and exclude the range of patterns in between.

Although we address a specific physical context, we believe that the main conclusions are general and relevant to other pattern-forming systems too. The vegetation context is particularly appealing because the mechanisms that induce the instabilities are well understood [4,5,11,12], and the ecological implications are significant, as they bear on pattern diversity which is a driver of biodiversity [13].

We study a simplified dimensionless version of the vegetation model introduced in Refs. [5,11], which still captures the infiltration and the uptake-diffusion feedbacks, and, therefore, nonuniform stationary instabilities to in-phase and antiphase patterns. The model consists of three fields: the areal density of the above-ground vegetation biomass $b(x,t)$, the areal density of soil water $w(x,t)$, and the areal density of the overland or surface water $h(x,t)$, which for a flat terrain satisfy the equations

$$b_t = g_b b(1 - b/\kappa) - b + \nabla^2 b, \tag{1a}$$

$$w_t = \mathcal{I}h - \nu w(1 - rb/\kappa) - g_w w + \delta_w \nabla^2 w, \tag{1b}$$

$$h_t = p - \mathcal{I}h + \delta_h \nabla^2(h^2), \tag{1c}$$

where $g_b = \nu w(1+\eta b)^2$, $g_w = \nu b(1+\eta b)^2$ are the rates of biomass growth and water uptake, respectively, and

$$\mathcal{I} = \alpha \frac{b + q(1-\phi)}{b+q} \tag{2}$$

is the infiltration rate. The infiltration feedback is captured by the biomass-dependent infiltration rate $\mathcal{I}$ and the transport term, $\delta_h \nabla^2(h^2) = -\nabla \cdot \mathbf{J}$, $\mathbf{J} = -2\delta_h h \nabla h$, in the equation for h, which describes overland flow along surface-water gradients induced by the high infiltration rates in vegetation patches. The strength of the infiltration feedback is controlled by the infiltration contrast parameter $\phi \in [0,1]$ and the water transport coefficient δ_h. The uptake-diffusion feedback is captured by the biomass-dependent water-uptake term $-g_w w$, which accounts for soil-water depletion in patches of growing vegetation, and

the diffusion term $\delta_w \nabla^2 w$, which accounts for soil-water diffusion towards these patches. The strength of this feedback is controlled by the parameter η, a measure for the root-to-shoot ratio, and by the soil-water diffusivity δ_w. Other model parameters include the precipitation rate p, the evaporation rate of soil water ν, reduction of evaporation by shading r, and "biomass diffusion" constant δ_b, which represents clonal growth or short-range seed dispersal. We refer the reader to the Supplemental Material [14] for the derivation of the simplified model, Eq. (1), and for the relations between the dimensionless quantities appearing in the model and their dimensional counterparts. More details about the original model can be found in Refs. [5,15].

Equation (1) have a nonzero stationary uniform solution that represents uniform vegetation. Both the infiltration feedback and the uptake-diffusing feedback can destabilize the uniform vegetation solution. This has been shown using models that capture only one of the two feedbacks [4,12] and is also shown in Fig. 1 using the model equations (1) that capture both feedbacks. Shown in the figure are results of a linear stability analysis carried out once when the infiltration feedback is switched off by setting the infiltration contrast to zero, $\phi = 0$ [Figs. 1(a), 1(b), and 1(c)], and once when the uptake-diffusion feedback is switched off by setting $\eta = 0$ [Figs. 1(d), 1(e), and 1(f)]. In both cases, the destabilization of uniform vegetation occurs through a stationary nonuniform instability characterized by a real-valued eigenvalue attaining a maximal value at a finite wave number as the growth-rate curves shown in Figs. 1(a) and 1(d) indicate, but the periodic patterns that appear are different. When the instability is driven by the uptake-diffusion feedback, the soil-water content in a patch of denser biomass decreases, and the biomass and soil-water distributions are antiphase [Fig. 1(b)]. When the instability is driven by the infiltration feedback, the soil-water content in a patch of denser biomass increases because of the increased infiltration rate, and the distributions are in phase [Fig. 1(e)]. Figures 1(c) and 1(f) show the neutral stability curves for the uptake-diffusion and the infiltration feedbacks, respectively.

In general, the two feedbacks act in concert and may affect one another. We studied the interplay between the two feedbacks by exploring the instability threshold of the uniform state in a plane spanned by the parameters δ_w and ϕ that control the uptake-diffusion and infiltration feedbacks, respectively. Figure 2 shows the instability thresholds for different values of η. We recall that the parameter η controls the strength of the uptake-diffusion feedback (along with δ_w) and is used here to change the relative strength of the two feedbacks. Figure 2(a) shows the instability threshold for a relatively low η value for which the instability is driven by the infiltration feedback. As the monotonically increasing threshold line indicates, the alternative uptake-diffusion feedback counteracts the infiltration feedback by inducing soil-water diffusion from water-rich vegetation patches to their dryer neighborhoods and shifts the instability threshold to higher infiltration contrasts ϕ. Figure 2(c) shows the instability threshold for a relatively high η value for which the instability is driven by the uptake-diffusion feedback. In this case, the threshold line is monotonically decreasing, indicating that the alternative infiltration feedback promotes the instability by lowering down its threshold. This behavior can be understood as follows. A higher infiltration contrast results in the interception of more runoff in denser vegetation patches, which increases vegetation growth and soil-water uptake, and, therefore, facilitates the instability by the uptake-diffusion feedback.

At intermediate η values, both feedbacks are equally important, and the instability threshold line is no longer monotonic as Fig. 2(b) shows. High values of δ_w lead to an instability of the uniform vegetation state by the uptake-diffusion feedback and to the formation of an antiphase periodic pattern (point T_2 in the diagram). Low values of δ_w lead to an instability of the uniform state by the infiltration feedback and to the formation of an in-phase periodic

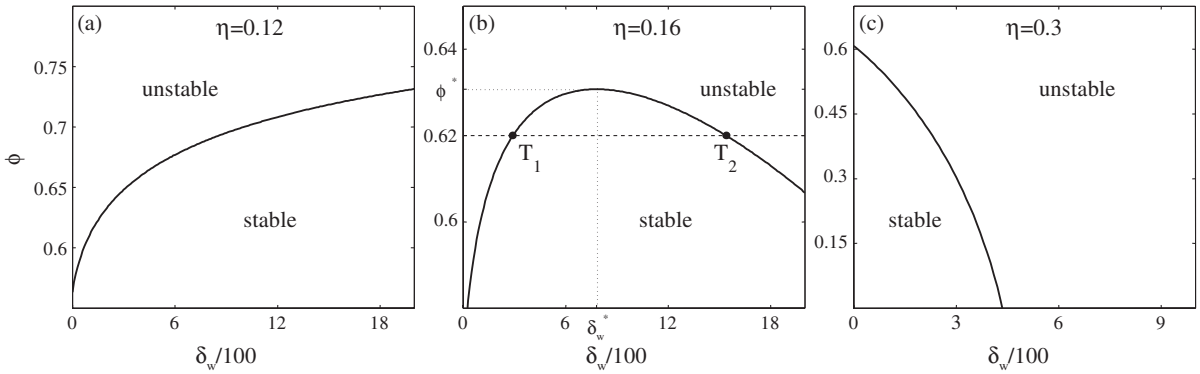

FIG. 2. Threshold lines for the nonuniform stationary instability of the uniform state at different η values representing (a) the dominance of the infiltration feedback (small value, $\eta = 0.12$), (c) the dominance of the uptake-diffusion feedback (large value, $\eta = 0.3$), and (b) comparable influence of the two feedbacks (intermediate value, $\eta = 0.16$). The threshold lines separate stability and instability domains of the uniform state as denoted. (δ_w^*, ϕ^*) denotes a codimension-two point. Parameters: $\delta_h = 10^4$.

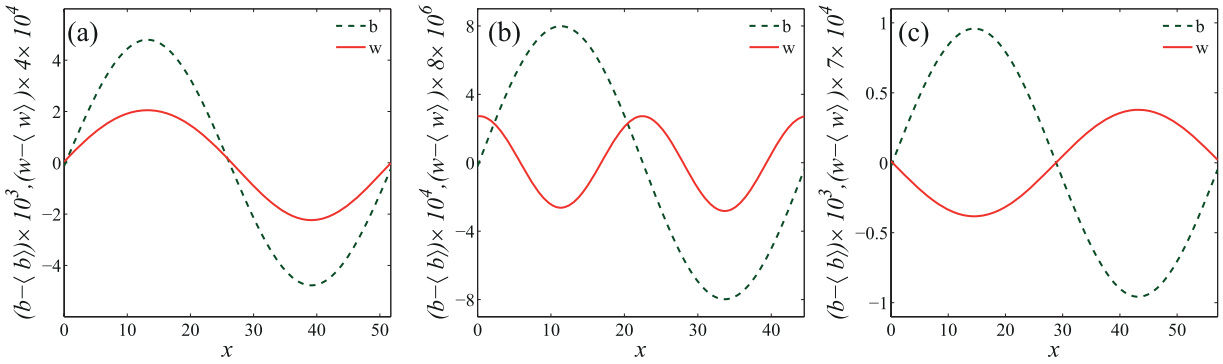

FIG. 3 (color online). The stationary periodic patterns that develop beyond the instabilities of the uniform state. Panels (a) and (c) show the in-phase and antiphase patterns obtained by instabilities driven by the infiltration and uptake-diffusion feedbacks, respectively. Panel (b) shows the rim pattern that results beyond the codimension-two point of the two instabilities.

pattern (point T_1 in the diagram). The instability at T_1 occurs despite the fact that the parameters that control it, ϕ and δ_h, are held constant. This is because of the counter-effect that the uptake-diffusion feedback has on the infiltration feedback.

Interestingly, we find that there is a particular point (δ_w^*, ϕ^*) in the (δ_w, ϕ) plane at which the instabilities at T_1 and at T_2 coincide, but, contrary to what one might expect, this is not a codimension-two bifurcation; the instability at (δ_w^*, ϕ^*) is a codimension-one bifurcation characterized by the growth of a single mode. As Fig. 3 shows, the growth of this mode results in a periodic pattern that is neither in-phase nor antiphase. We call this pattern a "rim pattern" because the soil-water distribution has maxima at the two rims of each biomass hump or patch.

To better understand the interplay between the two pattern-forming feedbacks away and in the vicinity of the point (δ_w^*, ϕ^*), we used a numerical continuation method to calculate the existence boundaries of periodic solutions with different wave numbers k, and numerical stability analysis (in 1d) to evaluate their stability thresholds. The results of this analysis for three different values of ϕ are shown in Fig. 4 in the form of "Busse balloons," i.e., as graphs of solution wavelength vs the control parameter δ_w [12]. The regions with crosses (circles) background [blue (green) shade online] denote the existence ranges of solutions representing in-phase (antiphase) patterns, and the dark shades denote the stability ranges of these solutions. When $\phi < \phi^*$ [Fig. 4(a)], the uniform state is stable for intermediate δ_w values and loses stability to antiphase (in-phase) patterns as δ_w is increased (decreased) past a threshold value. The Busse balloons associated with the two instabilities are separate, implying the existence of either in-phase patterns or antiphase patterns depending on the value of δ_w. When $\phi = \phi^*$ [Fig. 4(b)], the two Busse balloons touch one another at the codimension-two point,

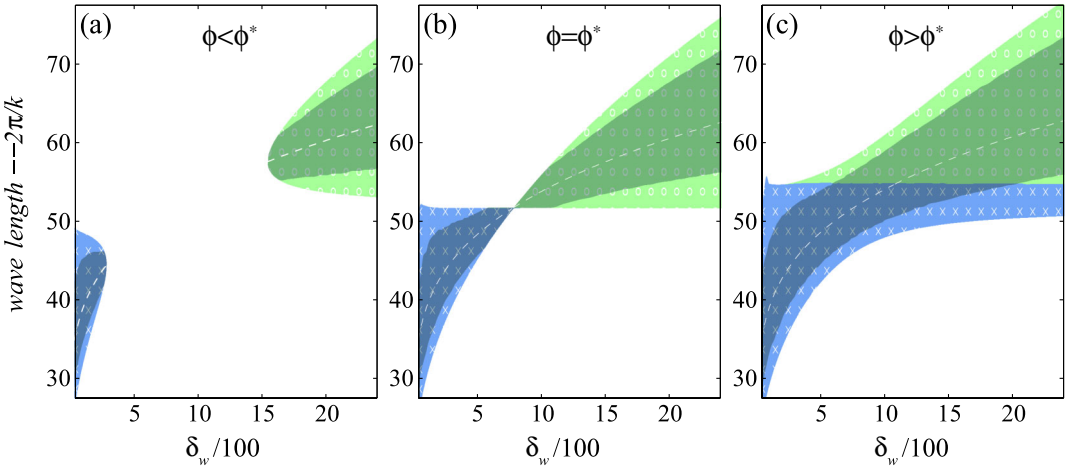

FIG. 4 (color online). Busse balloons of periodic solutions below ($\phi < \phi^*$), at ($\phi = \phi^*$), and above ($\phi > \phi^*$) the codimension-two point [see Fig. 2(b) for the definition of ϕ^*]. The region with crosses (circles) [blue (green) shade online] represents the existence range of in-phase (antiphase) solutions. The darker shades denote stable solutions. The dashed line denotes the wavelength that corresponds to the maximal growth rate as calculated by the linear stability analysis. The stability of the solutions was calculated using numerical linear stability analysis, where a domain length of $10L$ was taken (where $L = 2\pi/k$ is the wavelength of the solution).

and when $\phi > \phi^*$ [Fig. 4(c)], they overlap. As the dark shades indicate, there exists a continuous band of stable periodic patterns ranging from in-phase patterns at low wavelengths to antiphase patterns at high wavelengths that includes the rim pattern that is neither in-phase nor antiphase (dashed line). This pattern diversity is higher than the diversity of patterns that would have resulted from a codimension-two bifurcation (simultaneous growth of distinct in-phase and antiphase modes) because it includes all intermediate patterns.

The predicted multiplicity of stable biomass-water patterns ranging continuously from in-phase to antiphase patterns bears on the biodiversity of water-limited ecosystems. Water-limited landscapes often consist of woody and herbaceous vegetation (e.g., shrubs and annuals). The woody species generally form spatial patterns of biomass and soil water to which the herbaceous community responds. The continuous range of the soil-water distributions formed by the multiplicity of stable woody patterns provides a wide variety of complementary habitats for herbaceous species. These habitats consist of water-rich areas and divide into three major classes: open areas between woody patches (antiphase pattern), woody-patch areas (in-phase patterns), and rims of woody patches (rim patterns). Landscapes in which all pattern types appear can accommodate high species diversity because they provide habitats that make various compromises in terms of exposure to light, nutrients, grazing, etc.

The merging of two independent modes into a single mode at a codimension-two point of two Turing instabilities can be found in other models too. As an example, we mention a three-variable reaction-diffusion model for an activator and two inhibitors that has been introduced to describe patterns in gas-discharge systems [16]. For this model to show the above behavior, we have to assume inversely coupled inhibitor diffusion coefficients so that the acceleration of one instability is accompanied by the deceleration of the other. These examples raise an interesting mathematical question: does the co-occurrence of two or more instabilities that share the same spectral properties (eigenvalues of the linear problem) necessarily imply a codimension-one bifurcation that involves the growth of a single mode? Studies of this question can shed light on the generality of the results reported here.

The research leading to these results has received funding from the European Union Seventh Framework Programme (FP7/2007-2013) under Grant No. 293825 and from the Israel Science Foundation under Grant No. 861/09.

*bel@bgu.ac.il

[1] C. Valentine, J. d'Herbes, and J. Poesen, Catena **37**, 1 (1999).
[2] V. Deblauwe, N. Barbier, P. Couteron, O. Lejeune, and J. Bogaert, Global Ecol. Biogeogr. **17**, 715 (2008).
[3] E. Meron, Ecol. Model. **234**, 70 (2012).
[4] M. Rietkerk, M. C. Boerlijst, F. van Langevelde, R. HilleRisLambers, J. van de Koppel, L. Kumar, H. H. T. Prins, and A. M. de Roos, Am. Nat. **160**, 524 (2002).
[5] E. Gilad, J. von Hardenberg, A. Provenzale, M. Shachak, and E. Meron, J. Theor. Biol. **244**, 680 (2007).
[6] We distinguish here between a "codimension-two point" and a "codimension-two bifurcation." The former term denotes a point in the plane spanned by two control parameters where two instabilities coincide, whereas the latter term refers to a codimension-two point where the coincidence of the two instabilities gives rise to the growth of distinct modes.
[7] A. DeWit, D. Lima, G. Dewel, and P. Borckmans, Phys. Rev. E **54**, 261 (1996).
[8] M. Tlidi, P. Mandel, and M. Haelterman, Phys. Rev. E **56**, 6524 (1997).
[9] S. Ciliberto and J. P. Gollub, Phys. Rev. Lett. **52**, 922 (1984).
[10] E. Meron, Phys. Rev. A **35**, 4892 (1987).
[11] E. Gilad, J. von Hardenberg, A. Provenzale, M. Shachak, and E. Meron, Phys. Rev. Lett. **93**, 098105 (2004).
[12] S. van der Stelt, A. Doelman, G. Hek, and J. D. M. Rademacher, J. Nonlinear Sci. **23**, 39 (2013).
[13] M. Shachak *et al.*, *Biodiversity in Drylands: Towards a Unified Framework* (Oxford University Press, New York, 2005), pp. 3–14.
[14] See the Supplemental Material at http://link.aps.org/supplemental/10.1103/PhysRevLett.112.078701 for the derivation of the simplified model, Eq. (1), and for the relations between the dimensionless quantities appearing in the model and their dimensional counterparts.
[15] E. Meron, Math. Mod. Nat. Phenom. **6**, 163 (2011).
[16] M. Bode, A. W. Liehr, C. P. Schenka, and H. G. Purwins, Physica (Amsterdam) **161D**, 45 (2002).